Visual Abstract

Effect of Ti addition and cast part size on solidification structure and mechanical properties of medium carbon, low alloy cast steel

N. E. Tenaglia, D. O. Fernandino, A. D. Basso
INTEMA, Universidad Nacional de Mar del Plata-CONICET, Av. Colón 10850, Mar del Plata, B7606BVZ, Argentina
ntenaglia@fi.mdp.edu.ar, http://orcid.org/0000-0001-6372-88816372-8881
dfernandino@fi.mdp.edu.ar, https://orcid.org/0000-0003-4647-2663
abasso@fi.mdp.edu.ar, https://orcid.org/0000-0002-6167-4426

ABSTRACT. In this work, the effect of Ti addition and the cast part size on the solidification structure and mechanical properties of a medium carbon, low alloy cast steel was analyzed. The experimental analysis involved the design of the melts by using Thermo-Calc® software, where different amounts of Ti added to a standard chemical composition of an AISI 13XX steel were simulated. Then, the solidification macrostructure (dendritic pattern and grain size) and microstructure were characterized by using conventional and specific metallographic techniques. Finally, the mechanical behavior in terms of hardness and tensile properties were evaluated.
The results show that the addition of 0.12% of Ti promotes a fine dispersion of Ti nitrides and carbides, but when the Ti concentration raises to 0.2%, the size of the Ti nitrides and carbides increases while its amount decreases. Ti nitrides and carbides particles act as nucleation sites for the precipitation of ferrite from austenite, and it was found that the addition of Ti in the higher concentrations refines the solidification macrostructure (dendritic pattern) for both cast part sizes evaluated.
Regarding mechanical properties, the addition of Ti does not significantly vary the ultimate tensile strength but reduces the total elongation for cast part sizes.

KEYWORDS. Cast steel; Solidification structure; Mechanical properties.

OPEN ACCESS

Citation: Tenaglia, N. E., Fernandino, D. O., Basso, A. D., Effect of Ti addition and cast part size on solidification structure and mechanical properties of medium carbon, low alloy cast steel, Frattura ed Integrità Strutturale, 62 (2022) 212-224.

Received: 01.08.2022
Accepted: 19.08.2022
Online first: 27.08.2022
Published: 01.10.2022

INTRODUCTION

In recent decades, there have been important advances in steel engineering due to the continuous need to respond to problems posed, for example, by the oil industry, in areas such as oil recovery and transmission, and by the automotive industry, focused on improving vehicle safety and fuel economy. These studies, mainly aimed at the optimization of the chemical composition and processing, have led to the development of steel families with different microstructures, showing a wide range of improved mechanical properties [1-2].
Most of the reported studies are centered in the determination of mechanical properties and wear performance of steels that have previously suffered a thermomechanical process, such as rolling and forging. However, many steel parts related

to automotive, mining and oil industries can be obtained through melting and casting processes, since these parts have complex geometries and variables thickness. It is widely recognized that cast and rough parts with the same chemical have different mechanical properties. The properties of cast pieces depend on their macro and microstructure, which are highly influenced by the chemical composition and part size.

Defects in cast parts have great influence on the mechanical properties. The most common defects are shrinkage cavities, trapped gas cavities, inclusions and microsegregation, and most of these defects accumulate at the last regions of liquid, called "last to freeze (LTF) zones". During solidification of steels, and due to the low solubility in solid phase, dendrite arms tend to reject inclusions and trapped gas to the remaining liquid, therefore they accumulate at the interdendritic zones. The same occurs with alloy elements: most of them have direct segregation and tend to accumulate in the LTF zones [3-4]. In addition, at the end of the solidification process, LTF zones are commonly surrounded by solid and, many times, it is not possible to compensate for the contraction caused by solidification and cooling. The result is some contraction cavities at micron scale, located at LTF zones.

In the case of large or heavy cast parts, the low cooling rate at thick zones promotes a higher concentration and size of defects. This is because the solidification takes a longer time and promotes the rejection of inclusions, trapped gas and alloy elements from solid phase (dendritic zones or "first to freeze - FTF zones") to LTF zones. In addition, since the dendritic secondary arm spacing depend on cooling rate, LTF zones have a large concentration of defects, being larger in large cast parts compared to small cast part sizes, which is detrimental to the mechanical properties [4-5].

It is widely recognized that a proper distribution of defects can improve the mechanical performance of cast parts [6]. However, this cannot be done through heat treatments after solidification, but it can be achieved by a refinement of the solidification structure, which can be obtained by using inoculants. Its use aims at reducing steel grain size by means of an increase of the number of sites for heterogeneous nucleation during solidification. This produces an improvement in the mechanical properties of the steel due to a finer microstructure and a better distribution of defects and alloys elements, leading to a more homogeneous microstructure [6-9].

It has been proved that the addition of low amounts of Ti on steels (<0.435 wt.%) can effectively refine the solidification structure [10]. During the melting process, the addition of Ti produces the precipitation of titanium nitrides (TiN) and carbides (TiC), which have high melting temperatures and are stable in the liquidus temperature of the steel, prior to solidification. The Ti (N, C) particles have a low disregistry with δ-ferrite and act as sites for heterogeneous solidification, increasing mainly the nucleation rate of δ-ferrite dendrites and leading to a finer microstructure [9-11].

This work is focused on analyzing the influence of Ti additions on medium-C, low alloy cast steels for two different cast part sizes: a standard 1" keel block (ASTM A703) and a heavy section part specifically designed to obtain a lower cooling rate during solidification. Particularly, the solidification macrostructure (dendritic pattern and grain size), microstructure and tensile properties are characterized.

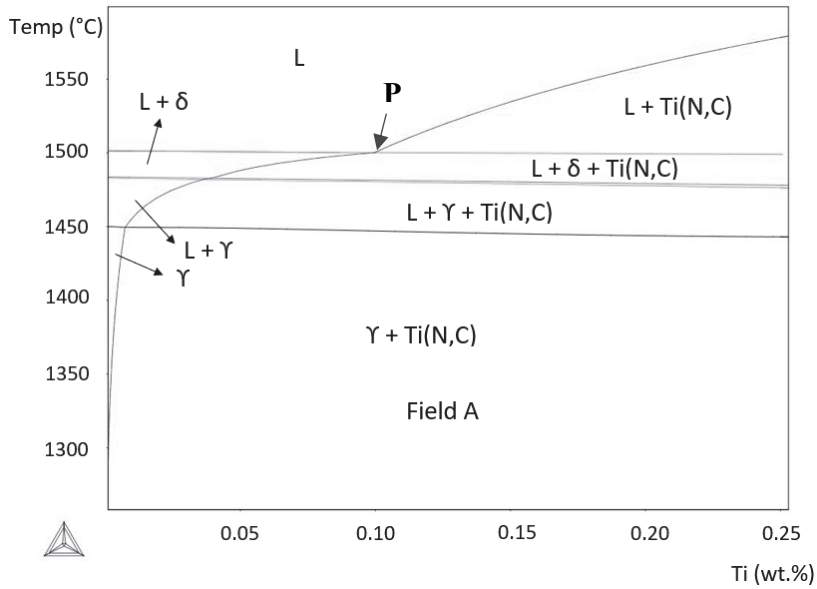

Figure 1: Simulated phase diagram for 0.27%C-0.7%Si-1.2%Mn-0.01N steel as a function of Ti added. (Wt.%)

DESIGN OF MELTS

The design of melts was performed by using the phase diagram retrieved from Thermo-Calc® software (based on CALPHAD-Computer Coupling of Phase Diagrams and Thermo-chemistry- and using the TCFE9 database, version 9), where different amounts of Ti added to a standard chemical composition of an AISI 13XX steel (0.27%C-0.7%Si-1.2%Mn-0.01N, wt.%) was evaluated. The AISI 13XX series is a common steel series used for producing cast parts [3]. The Fe-Ti phase diagram retrieved from Thermo-Calc® software is shown in Fig. 1. The diagram shows that for a Ti content from 0 to 0.1 wt.% approximately, Ti (C, N) are formed after the solidification of the primary phase, in this case δ-ferrite. For Ti content greater than 0.1 wt.%, the precipitation of Ti (C, N) occurs at a higher temperature, before the beginning of the solidification of δ-ferrite. Therefore, the chemical composition of the steels used were designed considering these results.

EXPERIMENTAL PROCEDURE

Material

The melts were prepared by an industrial foundry in a medium-frequency induction furnace of 500 kg capacity, using selected steel scrap and ferroalloys as raw materials (FeSi, FeMn, FeNi, FeTi). The steels were poured into sand moulds. The chemical composition was determined using a Baird DV6 spectrometer. The results of chemical compositions show a medium C, low alloy steel with standard chemical composition (steel A) and other two steels with the same base chemical composition but alloyed with a Ti content of 0.125 and 0.2 wt% for steel B and C respectively, as is listed in Tab. 1. It is worth noting that the Ti content of Steel A is a residual amount (<0.01wt%), and it is not considered alloyed.

Steel	C	Si	Mn	Ni	Ti	S	P
A	0.27	0.71	1.22	0.11	**<0.01**	0.002	0.013
B	0.26	0.70	1.19	0.10	**0.125**	0.002	0.013
C	0.27	0.68	1.18	0.10	**0.2**	0.002	0.013

Table 1: Chemical composition of the cast steels (wt.%).

Description of castings

Two different geometries of casting were used. The 1-inch keel block (1-inch KB), typically used for the characterization of cast steels (according to ASTM A703), and a heavy keel block (Heavy KB), which was specifically designed to obtain a significant lower cooling rate in the middle zone of the casting. The geometries and dimensions of both casting are schematized in Fig. 2. The geometrical parameters of both geometries at the location where samples were obtained are listed in Tab. 2. It is worthy to note that the volume of Heavy KB is 3.5 times greater than that for 1-inch KB and the thermal modulus is 2 times greater. This causes a significant difference in the cooling rate at the beginning and the end of the solidification, as was intended, which should cause great differences in the solidification structure of each sample.
The solidification and cooling processes of both castings were simulated using the software MagmaSoft®. In both cases, a filling temperature of 1595°C and "silica dry" moulds at 35°C were selected. Tab. 2 shows the geometrical parameters of the samples, as volume, surface and thermal modulus of the cast parts. In addition, table shows some thermal parameters obtained at the location where samples will be obtained (Fig. 2):

- Solidification time: time interval between liquidus and solidus temperatures for a selected point.
- Cooling rate 1: cooling rate at the beginning of the solidification. It is calculated for a temperature 2°C above the liquidus temperature. In this case, it corresponds to a temperature of 1498°C.
- Cooling rate 2: cooling rate at the end of solidification. It is calculated at the solidus temperature plus 10% of the [liquidus-solidus] temperature range. In this case, it corresponds to 1403°C.

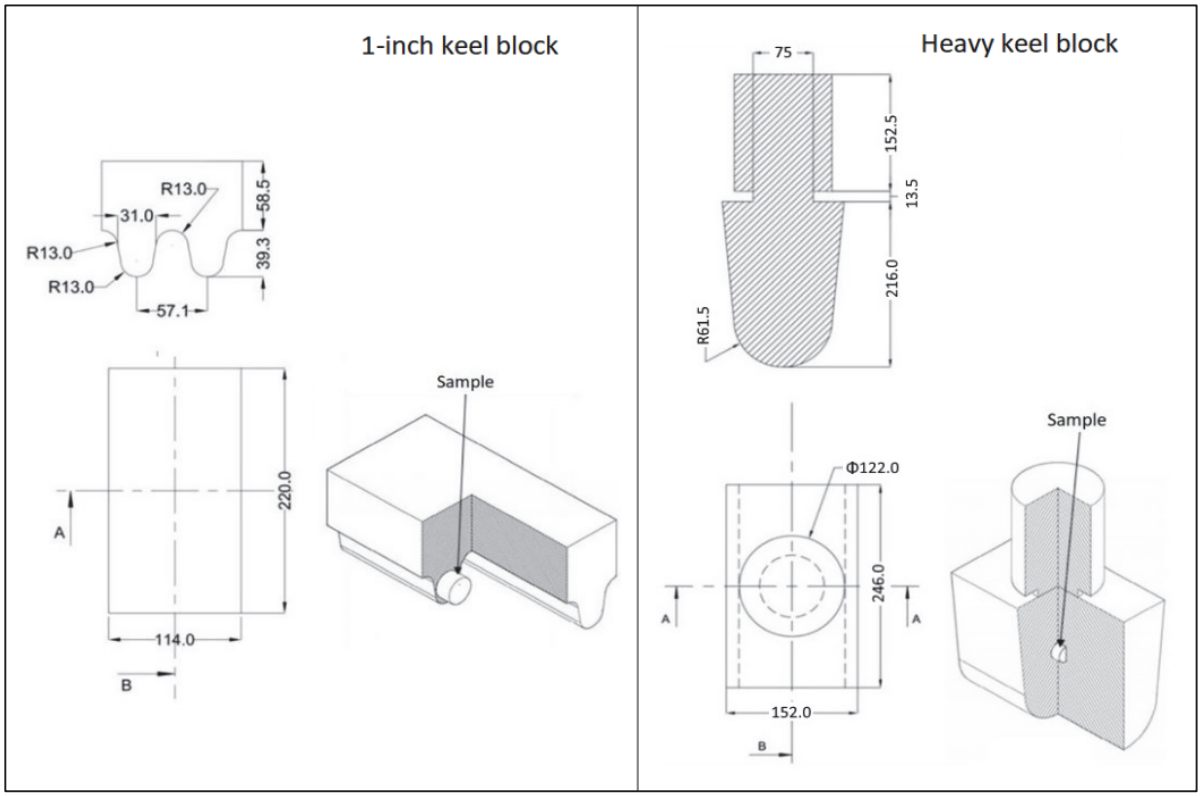

Figure 2: Geometries of cast parts. Dimensions expressed in mm.

Parameters	1-inch KB	Heavy KB
Volume [m³]	0.0019	0.0064
Surface [m²]	0.116	0.213
Thermal modulus [m]	0.016	0.03
Solidification time [s]	725	3106
Cooling rate 1 [°C/s]	0.31	0.029
Cooling rate 2 [°C/s]	0.162	0.048

Table 2: Thermal parameters of both cast geometries used.

Solidification structure characterization and mechanical properties

Samples were extracted from castings, as shown in Fig. 2. Then the specimens were grounded and polished using conventional techniques and etched with several regents. The characterization of inclusions and Ti(C,N) was made on samples without etching, using light optical microscopy (LOM). The microstructure was revealed by nital etching (2%) and the dendritic pattern was revealed by Motz etching. This etchant is commonly used in cast iron to reveal the LFT and FTF zones [12-15] and it has been useful to reveal the dendritic structure in cast steels containing high-Si contents [16]. Color etching produces the deposition of thin oxide films on the metallic surface. The thickness of the films depends mainly on Si concentration, and because of the light interference phenomenon, different thicknesses produce different colors, allowing the identification of the Si segregation pattern. Further information about color etching can be found in references [12,16]. The degree of refinement of the solidification structure as a function of Ti concentration was determined by measuring the prior austenitic grain size (austenitic phase corresponding to field A in Fig. 1). The determination of the grain size was performed according to the ASTM E112 requirements and using the lineal intercept procedure. For this purpose, allotriomorphic and Widmanstätten ferrite were used as references for the location of grain boundaries, due to these phases nucleating and growing at the prior austenite grain boundaries. This procedure was only made in samples in which grain boundaries were clearly identified. In addition, the dendritic pattern was also characterized using the same method. In this case, the average size of the FTF zones (dendrite cores) was determined by means of counting the interception of LTF zones with random lines. Each reported value is a mean of 15 measurements.

Regarding mechanical properties, a hardness test and tensile test were performed. Brinell hardness was carried out in a bench tester using a 2.5 mm tungsten carbide ball and 187.5 kg load (HBW2.5/187.5). Tensile tests were performed using standard specimens according to the ASTM E8 procedure. For each condition (chemical composition and cast part size), three specimens were machined and tested, reporting the mean values of tensile strength, yield stress and elongation until failure.

RESULTS AND DISCUSSION

Microstructural characterization: Inclusions on 1-inch KB

Fig. 3 shows the unetched surfaces of steel A, B and C of 1-inch KB samples. Steel A (see Fig. 3a) presented globular oxide type inclusions and a small fraction of Ti(N,C) particles, as a consequence of the residual content of Ti in this steel (<0.01 wt.%). In particular, a density of ≈ 50 Ti(N,C) particles/mm² with a mean edge length of ≈2 μm is observed. Steel B showed also globular oxide type inclusions and a great number of Ti(N,C) particles, which are easily identified as they present orange coloration and faceted shape (see Fig. 3b). A concentration of ≈ 400 Ti(N,C) particles/mm² with an edge length of ≈ 3 μm were identified. Finally, Steel C showed considerable larger Ti particles with lower density (see Fig. 3c). Particularly, a mean of ≈ 200 inclusions/mm² with an edge size of ≈ 7 μm were observed. This change in the count/size of the Ti inclusions of the Steel B and C can be explained as follows. For higher Ti content, the solidification interval of the phases increases, as can be observed in Fig. 1. This produces that for Steel C, the precipitation of Ti particles occurs in a longer temperature interval, promoting the coarsening and/or coalescence of such particles in the liquid field of the steel (at longer temperature interval, higher solidification time). This behaviour was also reported by Ohno et. al. [9].

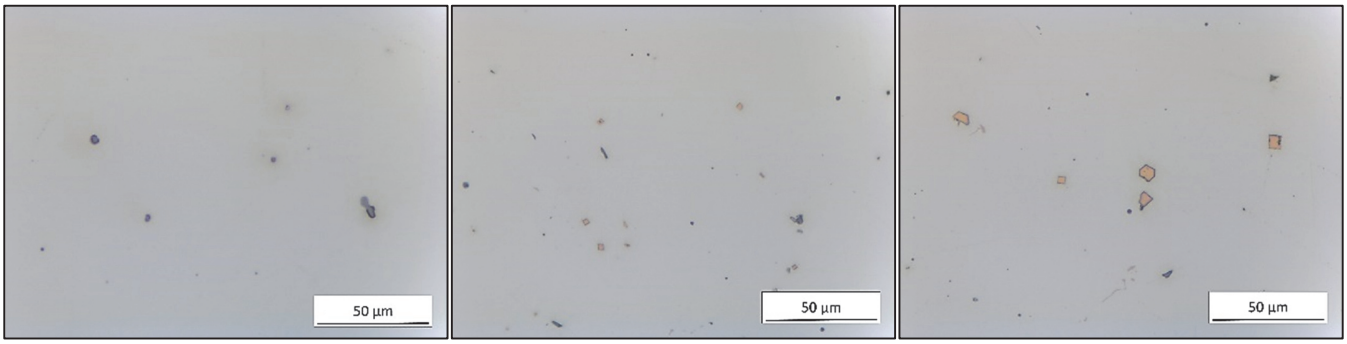

(a) (b) (c)

Figure 3: Unetched 1-inch KB samples. (a)Steel A, (b) steel B, (c) steel C.

Microstructural characterization: Inclusions on Heavy KB

The unetched surfaces of Heavy KB samples of steel A, B and C are shown in Fig. 4. Steels presented globular oxide type inclusions and Ti(N,C) particles, as was observed on 1-inch KB. In addition, every Heavy KB sample showed shrinkage micro cavities as shown in Fig. 4a. Particularly, Heavy KB samples corresponding to steels B and C showed the presence of micro cracks, as shown in Fig. 4b and c, which are occasionally attached to micro shrinkage cavities. Defects found in these samples could be associated with its large size. Low solidification cooling rates promotes the rejection of solute to LTF zones, which favours the growing of a large number of inclusions, including Ti(N,C) particles. On the other hand, LTF zones also presented micro shrinkage cavities since these are the last portions of material to solidify. The presence of micro cracks is attributed to the presence of micro cavities, which can work as stress concentrators and crack initiators. Moreover, the presence of hard and brittle particles is a preferential path for crack propagation. As the Ti content increases, larger Ti particles are formed, which promote the formation of micro cracks. All these defects are a consequence of the solidification and cooling processes and could be detrimental to mechanical properties.

Microstructure: 1-inch Keel Block

Fig. 5 shows the microstructure of 1-inch KB samples revealed by nital 2% for the steel A, B and C. In all cases, pearlitic-ferritic microstructure is observed, but significant differences about phases morphology, distribution and relative proportions were found. Steel A (Fig. 5a and b) showed a mainly pearlitic microstructure with allotriomorphic ferrite and some Widmanstätten ferrite located at prior austenite grain boundaries. Additionally, idiomorphic ferrite was also observed. The amount of ferrite in this sample was about 7.5% fraction in volume. Idiomorphic ferrite nucleates and grows mainly in

non-metallic inclusions and inside austenitic grains (Fig. 5b). The presence of idiomorphic ferrite allows to state that the prior austenitic grain is large. Steel B shows a microstructure like Steel A, Fig. 5c, but a larger amount of proeutectoid ferrite was measured. The addition of 0.12% of Ti raised the fraction of proeutectoid ferrite from ≈ 7.5% to ≈ 16%. These results agree with others results reported in the literature [17-18]. Finally, Steel C (Fig. 5d) showed a marked difference with Steel A and B, since it presented a ≈ 52% of proeutectoid ferrite (idiomorphic and allotriomorphic), four times higher than Steel B and eight times higher than Steel A.

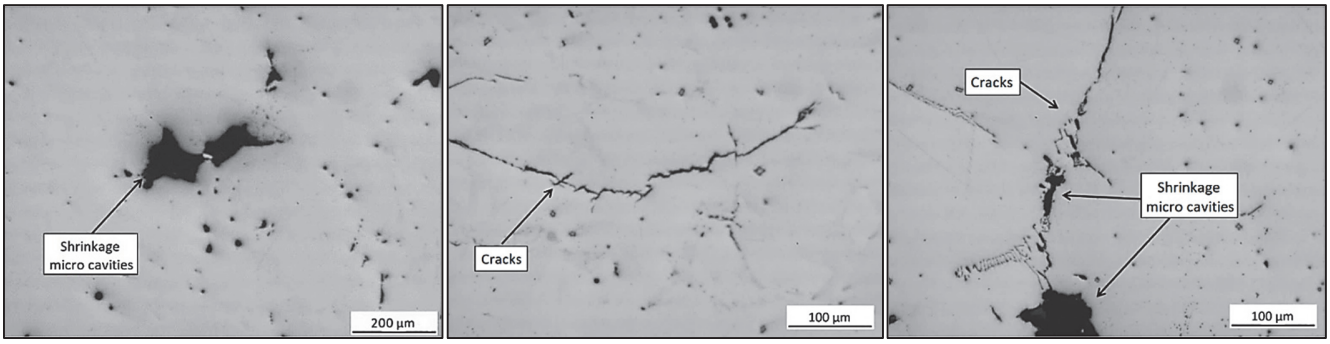

(a) (b) (c)

Figure 4: Unetched Heavy KB. (a) Steel A, (b) Steel B, (c) Steel C.

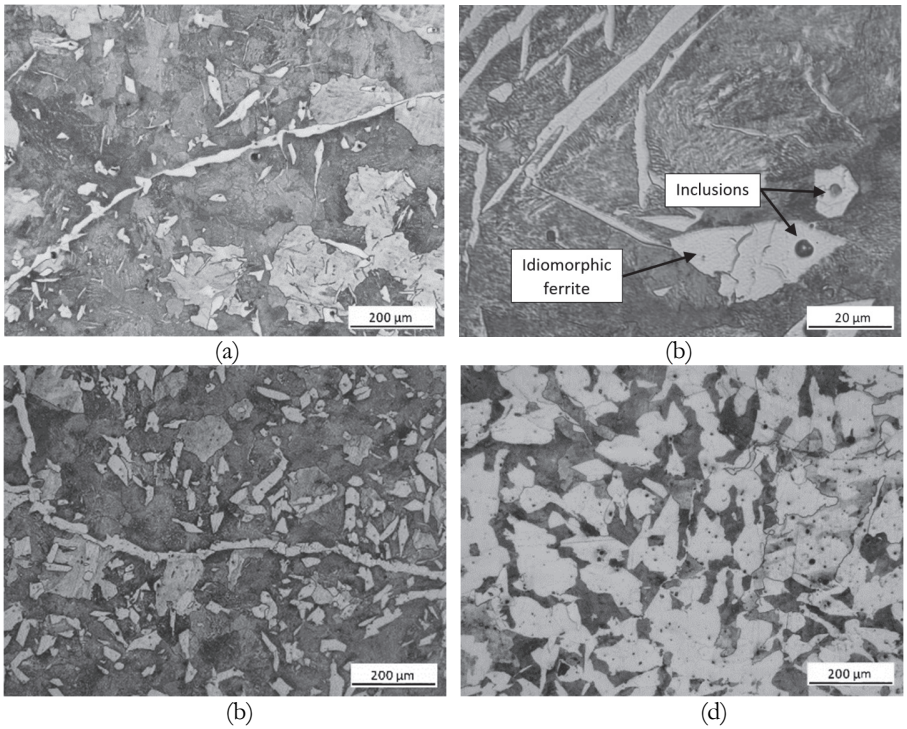

(a) (b)

(b) (d)

Figure 5: 1-inch KB microstructures. (a)(b) Steel A, (c)Steel B, (d)Steel C.

The differences in the proeutectoid ferrite percentage are attributed to two factors. First, Ti(N, C) particles act as nucleation sites for the precipitation of ferrite from austenite as is exemplified in Fig. 6, where a Ti(N,C) particles associated to idiomorphic ferrite in 1-inch KB sample of Steel B are observed. Second, the calculated phase diagrams for the Steel A, Steel B and Steel C show that the steels containing larger Ti contents have phase diagrams with larger ferritic fields [α or α+Ti(N,C)], which leads to a microstructure with larger amounts of proeutectoid ferrite (Fig. 7).

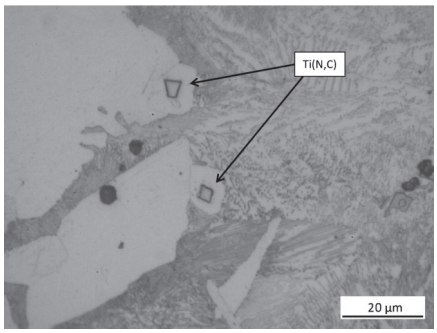

Figure 6: Idiomorphic ferrite associated with Ti inclusions. 1-inch KB - Steel B.

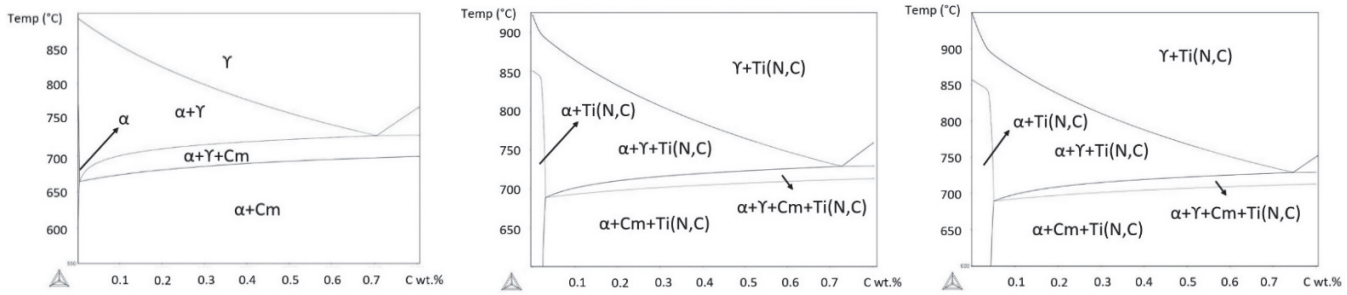

(a) (b) (c)

Figure 7: Ferritic/austenitic field as a function of Ti content. (a)Steel A–0.01%Ti, (b) steel B - 0.12%Ti, (c) steel C-0.2%Ti.

Heavy Keel Block

Compared to 1-inch KB, the Heavy KB also presented pearlitic-ferritic microstructures in as-cast condition, but the size and proportion of phases are different. The microstructures of Heavy KB are shown in Fig. 8. Steel A shows a percentage of proeutectoid ferrite about ≈ 53%, which is far from that observed in 1-inch KB-Steel A (≈ 7.5%). In addition, comparing Fig. 5a and Fig. 8a, proeutectoid ferrite size in Heavy KB is higher. For kinetic point of view, a low cooling rate in the solidification and cooling processes promotes a higher fraction and grain size of proeutectoid ferrite. For Heavy KB samples, the addition of 0.12 and 0.2% of Ti slightly raises the fraction of proeutectoid ferrite to ≈ 60 and 58.5%, and causes a significant reduction of proeutectoid ferrite size, as shown in Fig. 8b and Fig. 8c. Accordingly, for heavy section parts, the governing factor for the ratio ferrite/pearlite is the amount of Ti added; the cooling rate did not significantly modify the phase's proportion.

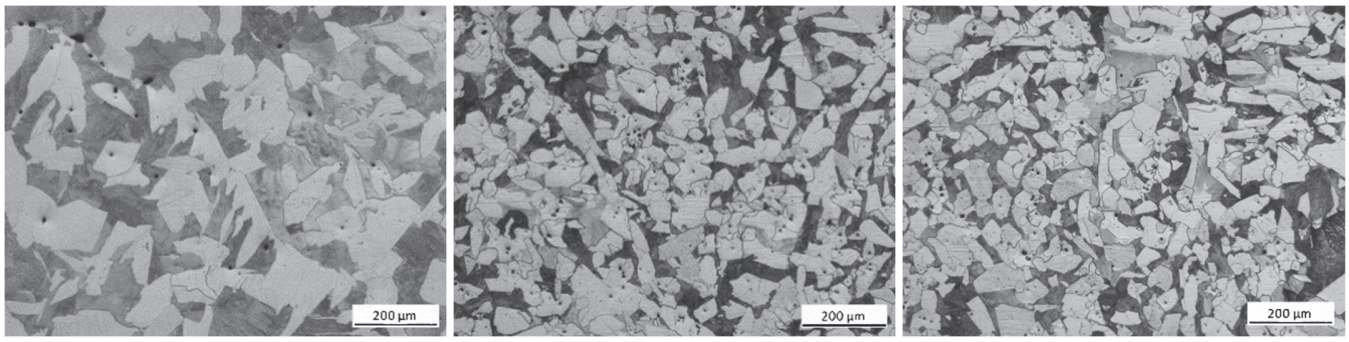

(a) (b) (c)

Figure 8: Heavy KB microstructures. (a)Steel A, (b) steel B, (c) steel C.

The percentages of proeutectoid ferrite in the microstructures, as a function of Ti content and cast part size is plotted in Fig. 9. The addition of Ti has a great influence on relative phases amounts in 1-inch KB samples. For larger part sizes, where the cooling rate is slower and closer to equilibrium, the addition of Ti shows a lower effect in the proeutectoid ferrite amount, but it does produce a phases refinement, especially on proeutectoid ferrite. For Steels B and C, Ti particles act as sites for nucleation of phases in solid state transformation (austenite to ferrite in this case), promoting a refining of the microstructure. It is worthy to note that the presence of higher amounts of proeutectoid ferrite in the microstructure in as-cast conditions could be highly beneficial for the manufacturing of mechanical components because: 1) it could increase the

machinability of pieces in as-cast condition and 2) the dimensional changes undergone by the parts when are subjected at a thermal cycle could be minimized [19].

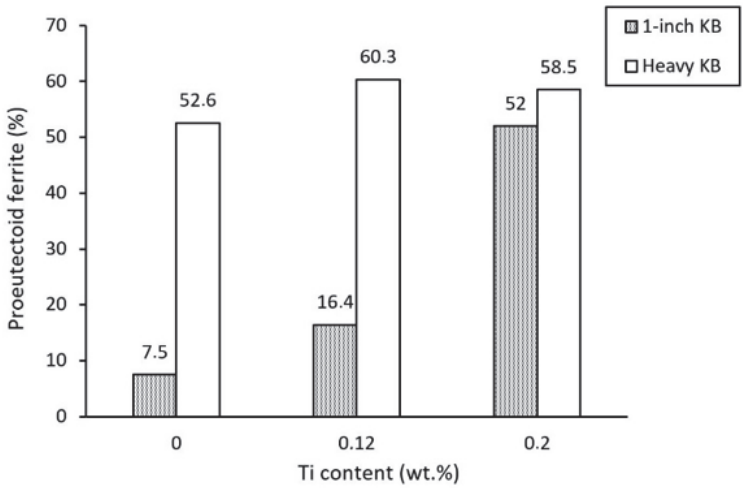

Figure 9: Proeutectoid ferrite fraction for the studied microstructures.

Macrostructure: Refinement of the austenitic structure

The effect of the Ti content as a refiner of the phases present in the as-cast microstructures was evaluated by determining the prior austenitic grain size. Since allotriomorphic and Widmanstätten ferrite nucleate and grow in austenitic grain boundaries, those phases were used as references to delimit the prior austenitic grain size. This measurement was only possible in 1-inch KB for Steels A and B, due to the other samples (Steel C) presented higher amounts of proeutectoid ferrite, making it hard to distinguish the ferrite corresponding to grain boundaries.

The austenitic structure of 1-inch KB- Steel A is shown in Fig. 10a. The surface was etched with Nital 2%. Several photos were taken using optical microscopy and then ensembled to cover a greater area. The macrostructure shows very large grains (of several millimetres), which are delimited by allotriomorphic and some Widmanstätten ferrite. Regarding to 1-inch KB – samples of Steel B (0.12% of Ti), the metallography observed in Fig.10B shows a higher number of grains of smaller size, with higher amount of acicular and idiomorphic ferrite, which has nucleated and grown in Ti particles and other inclusions. The results of the measurements of prior grain size are listed in Tab. 3. As a result, the sample corresponding to Steel A (0.01% of Ti) has a mean grain size of 1.84 mm, while the sample corresponding to Steel B (0.12% of Ti) has a grain size of 1.14 mm. This corresponds to a reduction in grain size of about 38%.

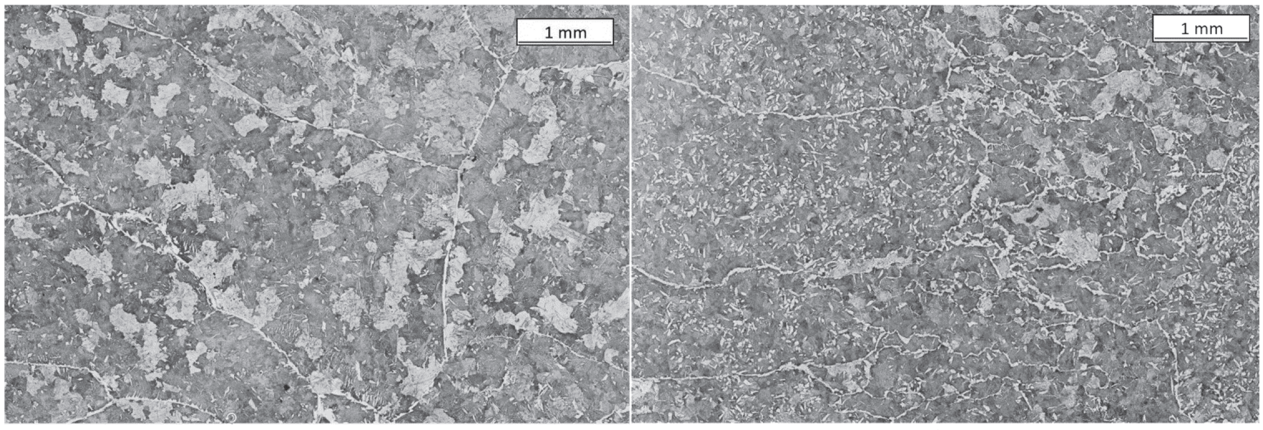

(a) (b)

Figure 10: Austenitic structure of 1-inch KB. (a) Steel A, (b) Steel B.

Macrostructure: Refinement of the dendritic structure

The application of Motz etching is exemplified in Fig. 11. Etching reveals a dendritic pattern that corresponds to the primary solidification of δ-ferrite dendrites, since in these steels the peritectic reaction during the solidification process occur. Fig.

11a corresponds to 1-inch KB sample for Steel A. The dendrite cores (FTF zones) are observed as brown and LTF zones as blue/green. Fig. 11b corresponds to the Heavy KB sample for Steel C. The dendrites are observed as orange color and LTF zones as green. The coloration of the surfaces depends mainly on silicon concentration and other factor, such as etching time, and etchant temperature. For this reason, the application of Motz etching looks different in the shown images, however it allows to clearly identify first and last to freeze zones.

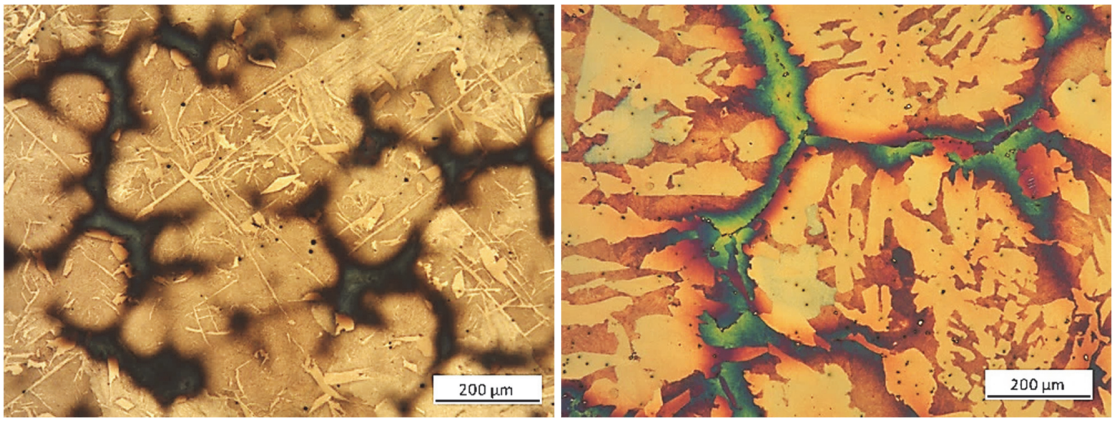

(a) (b)

Figure 11: Motz etching applied on: 1-inch KB (a) Steel A, (b) Heavy KB - Steel C .

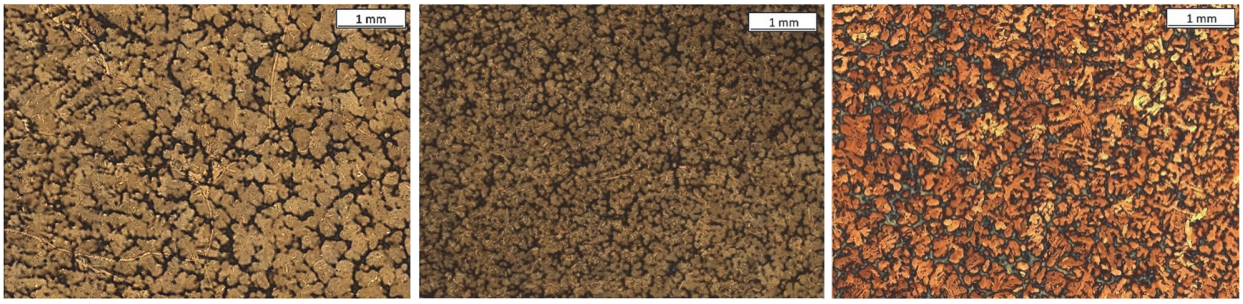

(a) (b) (c)

Figure 12: Dendritic pattern of 1-inch KB. (a) Steel A, (b) Steel B, (c) Steel C.

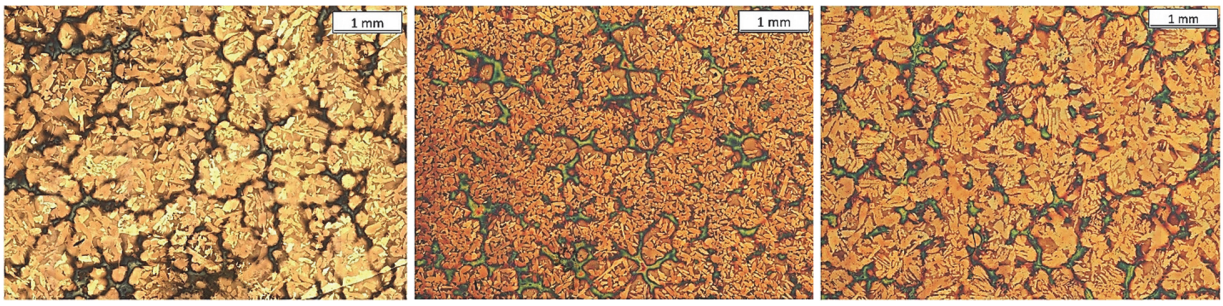

(a) (b) (c)

Figure 13: Dendritic patter of Heavy KB. (a) Steel A, (b) Steel B, (c) Steel C.

Fig. 12 shows the dendritic pattern of 1-inch KB for Steel A, B and C. Compared to Steel A, it is observed that the addition of 0.12% (Steel B) and 0.2% (Steel C) of Ti clearly refined the dendritic solidification structure, presenting smaller dendrites and more dispersed LTF zones. The modification of solidification macrostructure by means of Ti additions was also successful in the Heavy KB, as is shown in Fig. 13. Additionally, the size of FTF zone was also measured. The results of austenitic grain size and FTF measurements are listed in Tab. 3. For 1-inch KB, the macrostructure of Steel A has an average size of FTF zones of ≈ 0.39 mm, while the steel with 0.12% of Ti shown an average size of FTF zones of ≈ 0.25 mm, which corresponds to a reduction of about 30% of the original FTF zones size. However, the addition of 0.2% of Ti did not

introduce changes in the steel's macrostructure compared to Steel B (0.12% of Ti). The same behavior was found for Heavy KB, as can be observed in Fig. 13 and Tab. 3. This can be explained because despite the addition of 0.12% of Ti promotes a fine dispersion of Ti(N,C) particles, when the Ti concentration rises to 0.2%, the size of Ti(N,C) particles increases in size while its amount could decrease, losing your refiner effect. So, for the steel under study, the refining effect would be achieved for titanium concentrations higher than 0.1% (point P in Fig. 1). Similar results were reported by Ohno et. al. [11] for a 0.2%C cast steel.

Sample	%Ti	FTF zones size [mm]	Grain size[mm]
1-inch KB	<0.01	0.39	1.84
	0.12	0.27	1.14
	0.2	0.25	-
Heavy KB	<0.01	0.94	-
	0.12	0.66	-
	0.2	0.67	-

Table 3: Effect of Ti additions on grain and FTF zones size.

Mechanical properties: Hardness

The results of hardness measurements as a function of Ti content and cast part size are plotted in Fig. 14. The variation of hardness values can be explained by means of the competition of three phenomena: proeutectoid ferrite/pearlite ratio, phases size and the presence of hard Ti precipitates. In general, for the samples under study, the hardness increases as Ti content is higher. In the case of 1-inch KB, the highest hardness value of 232 HV corresponds to a Ti content of 0.12%. Despite having a large amount of proeutectoid ferrite, which would cause a decrease in the hardness value, the samples corresponding to 1-inch KB - Steel B showed a finer microstructure and the presence of dispersed Ti(N,C) hard particles, which cause an increase of the hardness. In the case of 1-inch KB with 0.2% of Ti, the large amount of proeutectoid ferrite and a similar density of Ti(N,C) particles promote lower hardness, compared to samples with 0.12% of Ti.

Regarding to Heavy KB, the addition of Ti caused an increase of the hardness values from 179 HV to 228 HV, which could be explain for both, the finer microstructures and the presence of Ti(N,C) particles. The hardness values for Steel B and C were similar (226HV and 228 HV respectively).

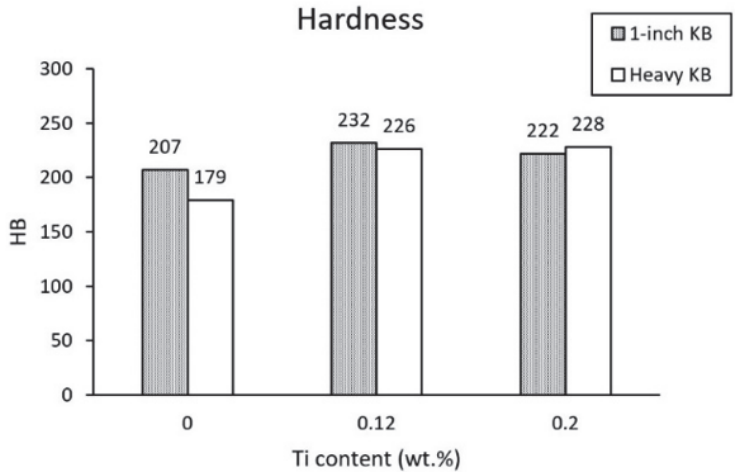

Figure 14: Hardness values as a function of cast part size and Ti content.

Mechanical properties: Tensile properties

The effect of Ti content and cast part size on tensile properties is plotted in Fig.15. In the case of 1-inch KB, the tensile strength was slightly modified with Ti additions. In agreement with the hardness, the highest value was obtained for the

Steel B (675 MPa). The presence of a majority pearlitic microstructure, dispersed Ti particles and a finer microstructure promote a higher tensile strength. The addition of Ti increased the yield stress from 421 MPa (0.01% of Ti) to 548 MPa (0.2% of Ti) but reduced the total elongation until failure from 15 to 5%. The increase in the yield stress values is related to the presence of micrometric and submicrometric titanium particles. It is widely known that the presence of second phase hard particles produces an increase in the hardness and yield stress due to dislocation fixing. This phenomenon is well known as "Precipitation Hardening". The reduction of ductility for larger Ti contents was also reported and corresponds to the presence of hard and brittle Ti(N,C) particles in the microstructure. Ti particles found along the grain boundaries or inside of grains greatly intensify the local stress concentration and increase the probability of cracks [18,20-21].

On the other hand, the improvement of mechanical properties in Heavy KB was not successful. As shown in Fig. 15, tensile strength does not present a clear dependence with Ti content. For all cases, the tensile strength is lower than the values corresponding to 1-inch KB (25-30% lower). The maximum value was 503 MPa for Steel C. As the Ti content increases, the yield stress decreases from 377 MPa to 257 MPa, which is opposite to the behavior of 1-inch KB. Total elongation is also decreased with Ti additions, but elongation values of Heavy KB are far from those for 1-inch KB. In this case, the total elongation values are lower than 3% in all cases. The behavior of Heavy KB can be explained by means of the analysis of the microstructures. It has been shown in Fig. 4 that, because of its large size and its slow solidification, Heavy KB samples presented a high number of inclusions, micro-voids and micro-cracks, which acts as stress concentrators. All these features decrease the mechanical properties, mainly the yield stress and total elongation. It is argued that the presence of this kind of defects has greater influence on tensile behavior of Heavy KB rather than the microstructure itself (phases, size and proportions). In fact, the results obtained from the tensile test for Heavy KB showed high dispersion.

Based on these results, for the case of heavy cast parts, the use of Ti as a refiner is not recommended, since it promotes the presence of a large amount of Ti(C,N) particles, which are detrimental to mechanical properties.

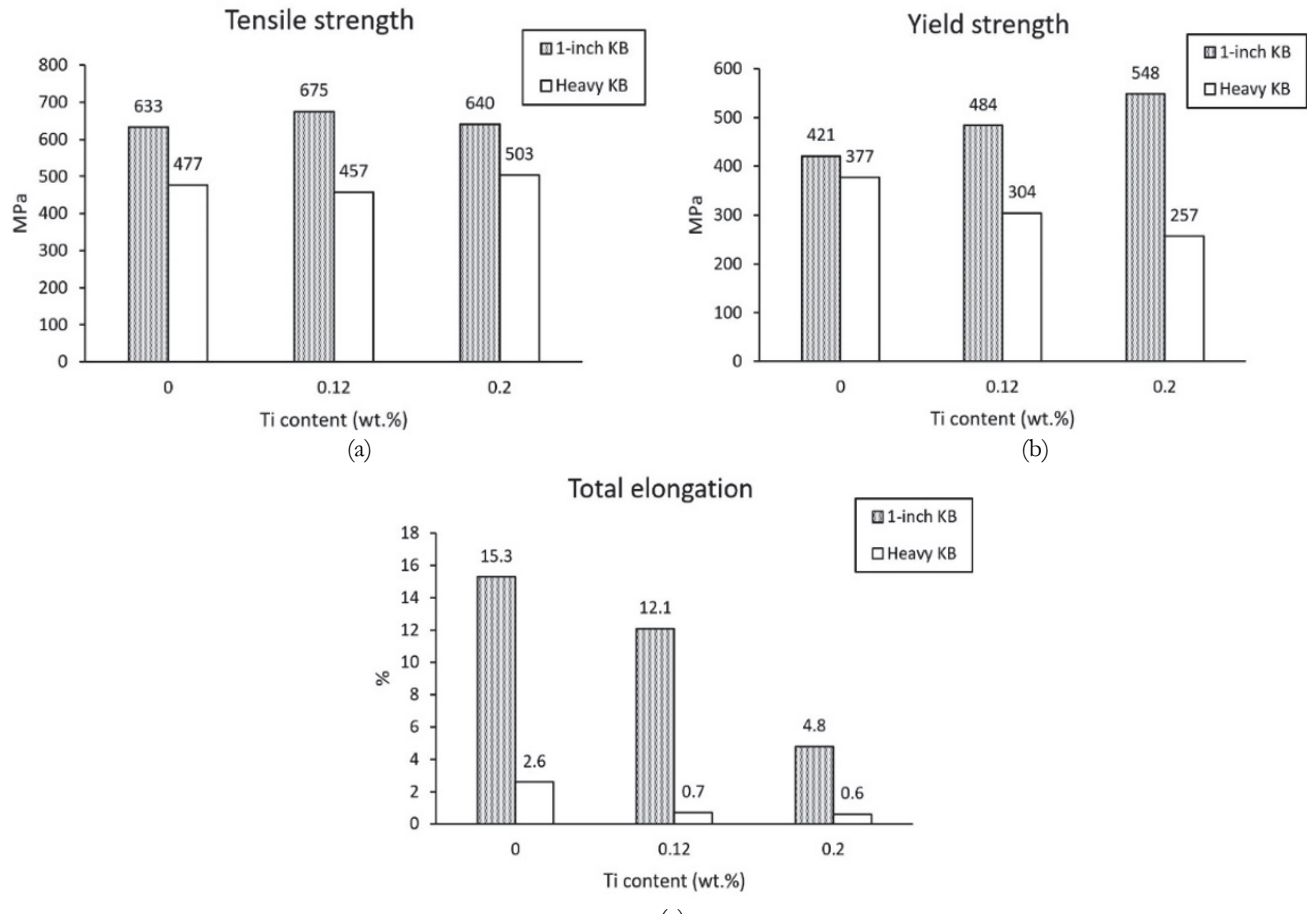

Figure 15: Effect of cast part size and Ti content in tensile properties. (a) Tensile strength, (b) yield strength, (c) total elongation.

CONCLUSIONS

The effect of Ti addition on a medium carbon, low alloy cast steel was evaluated for two different cast part sizes. The following are the main conclusions of this work:

- The addition of 0.12% of Ti on the chemical composition of a medium carbon, low alloy cast steel promotes a fine dispersion of Ti(N,C) particles. However, when the Ti concentration raises to 0.2%, the size of Ti(N,C) particles increases while its amount decreases, being this detrimental for the purpose of this work.
- The Heavy KB designed in this work showed a large number of inclusions (globular oxide type) and also micro cracks, some of them linking to micro shrinkage cavities.
- Ti increases the amount and decreases the size of proeutectoid ferrite on the as cast microstructures for the 1-inch Keel Block samples, since Ti(N,C) particles act as nucleation sites for the precipitation of ferrite from austenite. In the case of Heavy KB, Ti only refines the proeutectoid ferrite but does not increase its amount.
- The addition of Ti refines the dendritic pattern for both 1-inch and Heavy KB samples. The refinement is similar for 0.12 and 0.2 wt.% of Ti.
- The addition of Ti does not significantly vary the ultimate tensile strength but reduces the total elongation for both 1-inch and Heavy KB. In the case of 1-inch KB, Ti addition increases yield strength, while this property decreases with Ti concentration for Heavy KB.

REFERENCES

[1] Edmonds, D. V. (2010). Advanced Bainitic and Martensitic Steels with Carbide-Free Microstructures Containing Retained Austenite. In Materials Science Forum 638–642, pp. 110–117. DOI: 10.4028/www.scientific.net/msf.638-642.110.

[2] Matlock, D.K., Speer, J.G., Moor, E.D., & Gibbs, P. (2012). Recent developments in advanced high strength sheet steels for automotive applications: An overview. JESTECH. 15, pp. 1-12.

[3] Metals Handbook (1990). Properties and selection: Iron, Steels and High performance alloys. ASM, 1, p. 373.

[4] Krauss, G. (2003). Solidification, segregation, and banding in carbon and alloy steels. Metall Mater Trans B 34, pp. 781–792. DOI:10.1007/s11663-003-0084-z.

[5] Fredriksson, H., Akerlind, U. (2012). Solidification and Crystallization Processing in Metals and Alloys. Royal Institute of Technology, Stockholm, Sweden. pp. 550-551.

[6] Chen, X., Li, Y. (2006). Effects of Ti, V, and rare earth on the mechanical properties of austempered high silicon cast steel. Metall Mater Trans A 37, pp. 3215–3220. DOI: 10.1007/BF02586156.

[7] Cheng, X., Li, Y. (2007). Fracture toughness improvement of austempered high silicon steel by titanium, vanadium and rare earth elements modification. Materials Science and Engineering A 444, pp. 298-305. DOI: 10.1016/j.msea.2006.08.113.

[8] Fu, H., Qu, Y., Xing, J. (2009). Investigation of Solidification Structures of High Carbon Low Alloy Cast Steel Containing Re-V-Ti. Journal of Materials Engineering and Performance 18, (4), pp. 333-338. DOI: 10.1007/s11665-008-9202-z

[9] Ohno, M., Matsuura, K. (2008). Refinement of As-cast Austenite Microstructure in S45C Steel by Titanium Addition. ISIJ International 48 (10), pp. 1373–1379. DOI: 10.2355/isijinternational.48.1373.

[10] Sasaki, M., Matsuura, K., Ohsasa, K., Ohno, M. (2009). Refinement of As-cast Austenite Grain in Carbon Steel by Addition of Titanium. ISIJ International 49, (9), pp. 1362–1366. DOI: 10.2355/tetsutohagane.94.491.

[11] Ohno,M., Murakami, Ch.,Matsuura, K., Isobe, K. (2012). Effects of Ti Addition on Austenite Grain Growth during Reheating of As-Cast 0.2 mass% Carbon Steel. ISIJ International 52 (10), pp. 1832–1840. DOI: 10.2355/isijinternational.52.1832.

[12] Rivera, G., Boeri, R., Sikora, J. (1995). Revealing the solidification structure of nodular iron. Int J Cast Met Res. 8, pp. 1–5. DOI: 10.1080/09534962.1995.11819186.

[13] Fernandino, D.O., Boeri, R.E. (2019). In-situ microscopic analysis of ferritic ductile iron during tensile loading. Relation between matrix heterogeneities. Fatigue Fract Eng Mater Struct. 42, pp. 2220–2231. DOI:10.1111/ffe.13030.

[14] Fernandino, D.O., Tenaglia, N., Di Cocco, V., Boeri, R., Iacoviello, F. (2020). Relation between microstructural heterogeneities and damage mechanisms of a ferritic spheroidal graphite cast iron during tensile loading. Fatigue Fract Eng Mater Struct. 43, (6), pp. 1262-1273. DOI:10.1111/ffe.13221.
[15] Fernandino, D.O., Boeri, R.E., Massone, J. (2018). Mechanism of Damage of Ferritic Ductile Iron, Influence of Matrix Heterogeneity. Materials Science Forum. 925, pp. 288-295. DOI: 10.4028/www.scientific.net/MSF.925.288.
[16] Tenaglia, N.E., Boeri, R.E., Basso, A.D., Massone, J.M. (2016). Macro and microstructural characterisation of high Si cast steels – Study of microsegregation patterns. Int J Cast Met Res. 30, (2), pp. 103-111. DOI: 10.1080/13640461.2016.1258515.
[17] El-Faramawy, H., Ghali, S., Eissa, M. (2012). Effect of Titanium Addition on Behavior of Medium Carbon Steel. Journal of Minerals and Materials Characterization and Engineering 11. (11), pp. 1108-1112. DOI: 10.4236/jmmce.2012.1111118.
[18] Rassizadehghani, J., Najafiy, H., Emamy, M., Eslami-Saeen, G. (2007). Mechanical Properties of V-, Nb-, and Ti-bearing As-cast Microalloyed Steels. J. Mater. Sci. Technol. 23(6).
[19] Echeverría, M.D., Moncada, O.J., Sikora, J.A. (2001). Influence of the dimensional change, and its dispersion, on the fabrication size tolerances of austempered ductile iron (ADI) parts: comparison with SAE 4140 steel. ISIJ International, 41(1), pp. 25–30. DOI: 10.2355/isijinternational.41.25.
[20] Xu., G., Gan, X, Ma,G., Luo, F., Zou, H. (2010). The development of Ti-alloyed high strength microalloy steel. Materials and Design 31, pp. 2891–2896. DOI: 10.1016/j.matdes.2009.12.032.
[21] Kang, Y. Mao, W.M., Chen, Y.J., Jing, J., Cheng, M. (2016). Effect of Ti content on grain size and mechanical properties of UNSS44100 ferritic stainless steel. Materials Science & Engineering A 677, pp. 211–221. DOI: 10.1016/J.MSEA.2016.08.070.